

Doctoral School of Material Sciences and Technologies

MODELING LEAD-FREE INTERCONNECT RELIABILITY UNDER CREEP IN ADVANCED PACKAGING.

Dissertation Booklet

OE-BGK Student's name: Ramiro Sebastian Vargas Cruz

ATDI Registration number: T000382/FI12904/D

2025 Supervisor's name: Viktor Gonda

1. Introduction (Chapter 1)

In materials science, creep is defined as the time-dependent plastic strain at a constant stress above the melting temperature (T_m). Since creep involves plastic (irreversible) deformation, its application is highly relevant to material reliability. The material selected for this work was soldering compositions since their importance in electronics is essential.

While compiling information regarding soldering materials, it was found that specific regulations on Waste from Electrical and Electronic Equipment (WEEE) and Restrictions on Hazardous Substances (RoHS) have limited the usage of Pb (lead) in electronic applications. Therefore, lead-free soldering materials became the main scope of this research. Certainly, the new lead-free compositions implied a different melting temperature that must be considered in manufacturing and failure prediction. Some of the most relevant parameters for soldering material selection are listed in **Table 1**

Table 1. Important properties of solder alloys.

Table 1. Important properties of solder alloys.					
Properties relevant to manufacturing	Properties relevant to reliability and performance				
 Melting/liquidus temperature Wettability (of copper) Cost Environmental friendliness Availability and number of suppliers Manufacturability using current processes Ability to be made into balls Copper pick-up rate Recyclability Ability to be made into paste 	 Electrical conductivity Thermal conductivity Coefficient of thermal expansion Shear properties Tensile properties Creep resistance Fatigue properties Corrosion and oxidation resistance Intermetallic compound formation 				

The novel lead-free soldering materials had to meet certain mechanical endurance and electrical performance conditions. Some of the most common applications and thermal service ranges are listed in **Table 2**.

Table 2. Thermal environments for solder in several electronic packages.

Use conditions	Thermal e	xcurs	ion (°C)
Consumer electronics	0	to	60
Computers	15	to	60
Telecommunications	-40	to	85
Commercial aircraft	- 55	to	95
Military aircraft	- 55	to	125
Space	-40	to	85
Automotive – Passenger compartment	-55	to	65
Automotive – Under the hood	- 55	to	150

2. Outline of the Dissertation

The work presented in this dissertation has been divided into four chapters.

2.1 Chapter 2. Fundamental thermal-mechanical behavior of soldered Stacks

The following chapter examines the thermal-mechanical creep behavior and structural integrity of electronic packages that contain solder joints. A Finite Element Model (FEM) was developed to simulate thermal cycling loads on a simplified package configuration, employing the Anand material model to characterize the creep behavior of the solders. Stress and strain analyses were conducted for the three types of lead-free solders, providing a comparative assessment of their mechanical responses. The results highlight the importance of understanding the mechanical behavior of lead-free solders to ensure the durability and integrity of electronic assemblies.

2.1.1 Simulation Setup

The following case study compares the equivalent creep strain and stress of three lead-free solders with those of eutectic thin-lead solder. The modelled 2-D cross-section presented in Figure 1 emulates a flip chip assembly. This model is part of the example list of the simulation software used for this research – MSC Marc Mentat Studio.

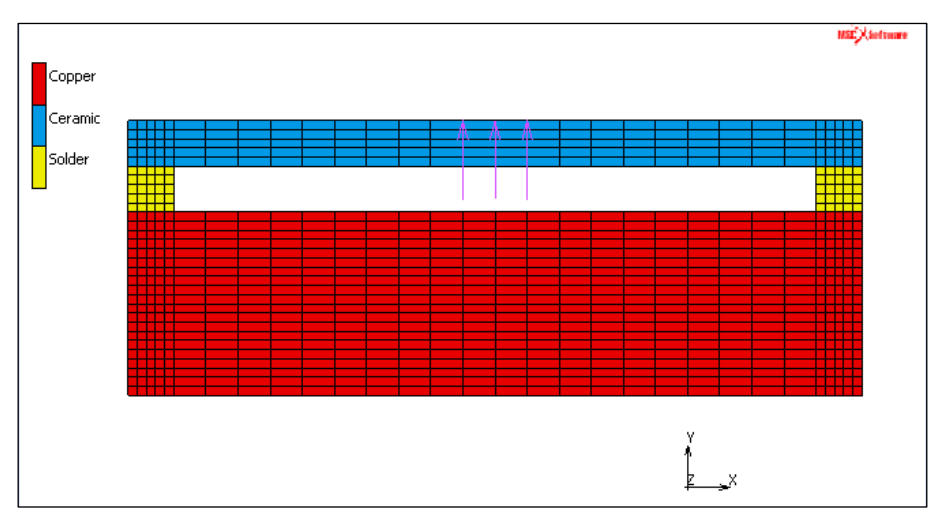


Figure 1. Flip-Chip Structural setup and materials description of the sample.

As this research describes creep behavior using the Anand Model, viscoplastic properties must be established. The elastic-plastic parameters for the eutectic SnPb solder, as well as for the three lead-free solders of interest, are detailed in Table 3. The Melting Temperature (T_m) was included to highlight the considerable variation between eutectic SnPb and unleaded solders (over 30°C). Additionally, Anand's parameters are listed in Table 4.

Table 3. Thermomechanical properties.

Material	T range (°C)	E (GPa)	ν	α (ppm/°C)	T_m (°C)
Sn3.5Ag	20 – 150	48 - 25	0.40	20.2 - 21.7	221
SAC 305	25 - 125	90 - 38	0.42	16 - 22.4	217
SAC 387	20 - 100	46 - 35	0.40	17.6	217
SnPb	25 - 125	22 - 12	0.40	21	183
Cu	_	1.3	0.34	17	1084
Ceramic	_	0.375	0.22	5.36	_

Table 4. Material parameters for Anand model.

Description	Sn3.5Ag	SAC 305	SAC 387	SnPb
s_0 (MPa)	0.65	21	37.1	56.33
$A(s^{-1})$	344.716	3 501	65.92	$1.49 \cdot 10^7$
ξ	3	4	8	11
m	0.143	0.25	0.346	0.303
h_0 (MPa)	23 241	180 000	86 442.8	2 640.75
ŝ (MPa)	26	30.2	80.8	80.42
n	0.0447	0.01	0.0002	0.0231
a	1.46	1.78	1.29	1.34
$Q\left(J\cdot \text{mol}^{-1}\right)$	54 364	77 490.78	55 307.8	90 040

The model was subjected to a thermomechanical load. The mechanical load consisted of a four-cycle sinusoidal oscillation with an amplitude of 0.5 mm, running for 120 s, as shown in Figure 2. Simultaneously, a thermal load that changes the temperature of the entire sample from 0 to 125°C is also applied, describing two cycles (Figure 3).

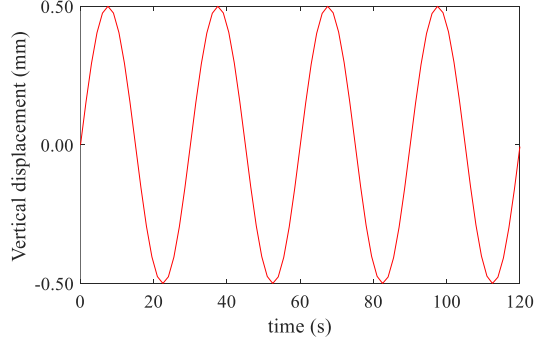


Figure 2. Sinusoidal Structural: Displacement vs Time.

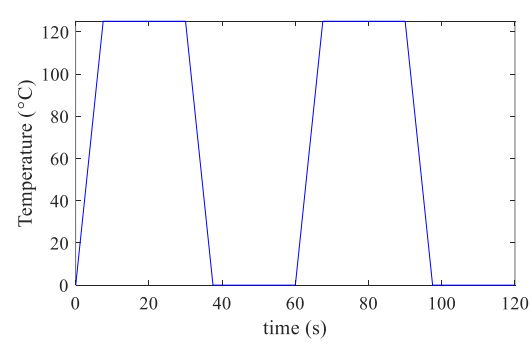


Figure 3. Thermal load: Temperature vs Time.

Restrictions regarding displacement and rotation in all three axes were applied to the bottom part of the sample, and a displacement restriction in the horizontal axis x was used on both sides of the model.

2.1.2 Results and Discussion

Average and maximum values of the Equivalent Creep Strain, as well as Total Equivalent Stress, are summarized in Table 5. Certainly, SAC305 shows the minimum average creep strain (4.8·10⁻³), whereas SnPb shows the maximum average value (12.1·10⁻³). On the other hand, regarding total equivalent stress, Sn3.5Ag shows the minimum average value (19.70 MPa), whereas SAC387 shows the maximum average value (39.38 MPa).

Table 5. Main values of equivalent creep and stress

		SnPb	Sn3.5Ag	SAC305	SAC387
Creep	Max	24.9	20.9	13.0	14.8
(10^{-3})	Av	12.1	7.03	4.80	5.64
Stress	Max	60.46	36.72	52.87	61.57
(MPa)	Av	33.57	19.70	34.66	39.98

2.1.3 Conclusions

From the equivalent creep strain comparison, it is evident that the mechanical load governs the creep behavior rather than the thermal load. From the results in terms of total equivalent creep strain, unleaded solders present a favorable value, nearly fifty percent less than that of the eutectic solder. SAC305 and SAC387 appear to have a high degree of similarity in terms of thermomechanical properties. However, the total equivalent creep strain of SAC305 is less than that of SAC387, with a final total equivalent creep strain of 0.12 and 0.14, respectively.

On the other hand, the total equivalent stress graph correlates with the thermal load, displaying two cycles. Regarding the total equivalent stress, Sn3.5Ag presents the minimum values, whereas SAC387 presents the maximum. Indeed, the curve described by the eutectic solder is not significantly different from that of the SAC solders. Additionally, the average stress of the eutectic solder is slightly less than that of the SAC305 and SAC387.

To summarize, lead-free solder materials exhibit lower creep strain curves under thermomechanical loads compared to eutectic SnPb solder. Yet, further analysis should be carried out to determine which one presents better performance in another time-dependent variable and still exhibits acceptable creep behavior.

2.2 Chapter 3. Effect of Anand parameters on the behavior of soldered stacks

SAC solder compositions have been considered the most suitable candidate to replace the eutectic Sn-Pb solder in many applications. Its reliability in terms of long-lasting work periods

is still widely analyzed. Some selected SAC compositions are detailed in Table 6. SAC solders have a relatively higher melting temperature (>217°C) than the eutectic Sn-Pb solder (183°C).

Table 6. Some typical SAC Solder Compositions.

Allow	Weight percentage - wt%		e - wt%
Alloy	Sn	Ag	Cu
SAC 305	96 - 97	2.8 - 3.2	0.3 - 0.7
SAC 387	95 - 96	3.6 - 4.0	0.5 - 0.9
SAC 405	95 - 96	3.8 - 4.2	0.3 - 0.7

The primary focus of this chapter is to refine the geometry model and assess the impact of various Anand parameters on SAC305 in simulation results. A summary of Anand parameters reported by several authors is shown in Table 7.

Table 7. Anand parameters for SAC305 in various sources.

	Year	2004	2009	2013	2015	2015	2018
	Author	Janz	Mysore	Herkommer	Basit	Lall	Alam
\mathbf{s}_0	MPa	45.9	2.15	1.0665	21	32.39	6.5
A	s^{-1}	5870000	17.994	1.43E+08	3501	1100	3700
ξ		2	0.35	1.472	4	6	4
m		0.0942	0.153	0.1414	0.25	0.39	0.47
h_0	MPa	9350	1525.98	5023.9	180000	174130	70000
s	MPa	58.3	2.536	20.2976	30.2	67.7	7.72
n		0.015	0.028	0.0324	0.01	0.0008	0.0315
a		1.5	1.69	1.12	1.78	1.75	1.9
Q	$J \cdot mol^{-1}$	62026.17	82895.56	88581.38	77491.14	33258	95616.75

A reliability approach is introduced in this research. Creep strain energy density is analyzed from the simulations. Additionally, a new set of lead-free soldering materials (SACX solders) is being considered for further comparison (Table 8).

Table 8. SAC-X material parameters for the Anand creep model.

Description	SACQ	SACR	InnoLot
<i>s</i> ₀ (MPa)	0.405	34.72	32.42
A (s ⁻¹)	$2.45 \cdot 10^{8}$	1000	25 000
ξ	0.068	6	7
m	0.36	0.15	0.35
h_0 (MPa)	3521.56	145 640	88 875
ŝ (MPa)	0.638	71.71	56.76
n	0.0056	0.001	0.0097
a	1.243	1.55	1.45
$Q\left(J\cdot \operatorname{mol}^{-1}\right)$	112 313.8	92290.52	13.9

2.2.1 Simulation Setup

For the finite element modeling, a 167GJJ Package from Texas Instruments was selected. This FO-WLP package includes a fine pitch Ball Grid Array (BGA). The main dimensions are shown in Figure 4 and Figure 5.

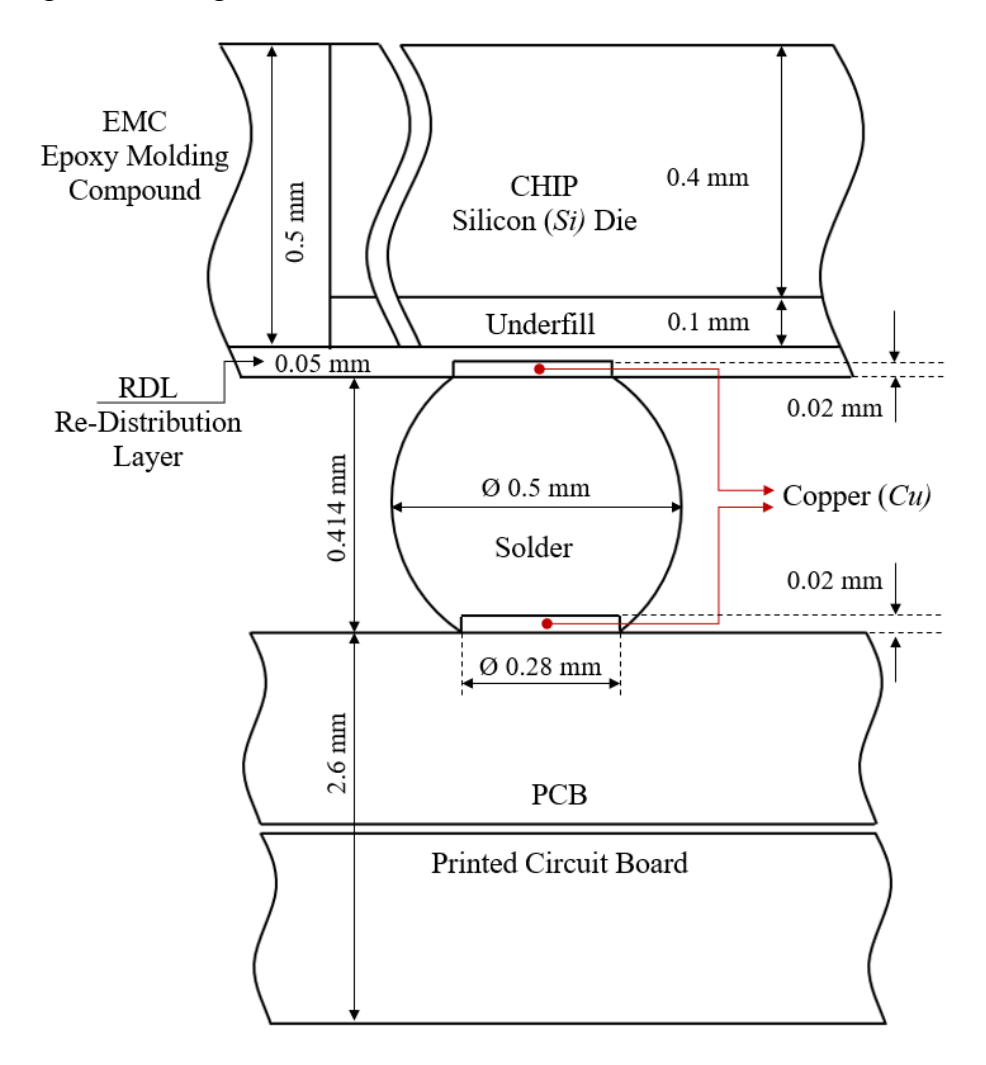


Figure 4. Flip-Chip Structural setup and materials description of the sample.

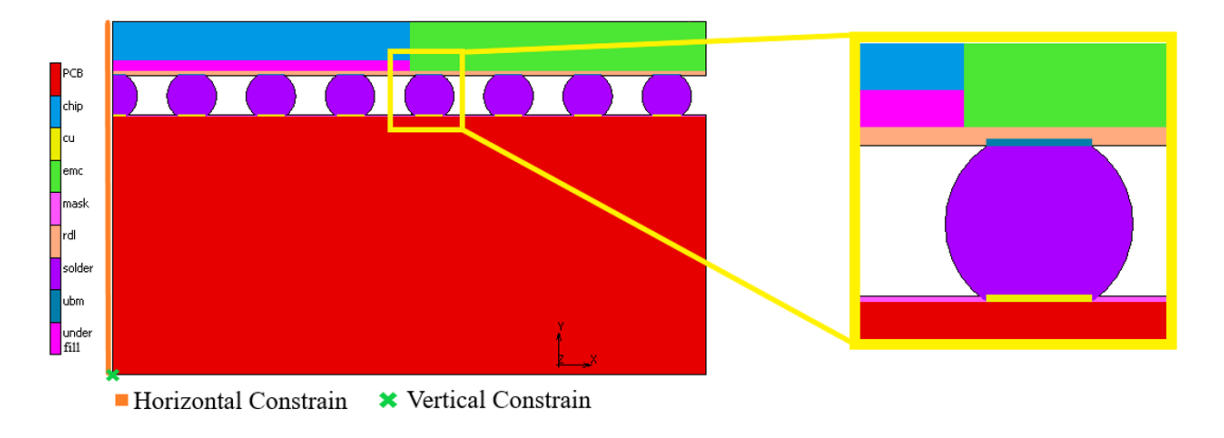


Figure 5. 2D Model (Half cross-section of the chip).

While Table 9 was used for most of the materials described in Figure 5, several replicates were run by changing the solder material properties taken from Table 7 and Table 8.

Tab	le 9	9. N	[aterial	parameters
-----	------	------	----------	------------

Table 9. Waterial parameters.							
Young's Modulus (GPa)	Poisson's Ratio	CTE ¹ (ppm/°C)	Tg ² (°C)				
131	0.3	2.8					
T < Tg: 18.5; T > Tg: 1.2	0.3	T < Tg: 9; T > Tg: 18	163				
T < Tg: 0.92; T > Tg: 0.1	0.3	T < Tg: 80 T > Tg: 227	205				
117	0.34	17					
T < Tg: 3.8; T > Tg: 0.125	0.3	T < Tg: 44; T > Tg: 119	141				
T < Tg: 2.4; T > Tg: 0.23	0.3	T < Tg: 60; T > Tg: 161	100				
For x,y: 25; For z: 11	For xy 0.11 for xz, yz 0.39	For x, y: 15 For z: 46					
	Young's Modulus (GPa) 131 T < Tg: 18.5; T > Tg: 1.2 T < Tg: 0.92; T > Tg: 0.1 117 T < Tg: 3.8; T > Tg: 0.125 T < Tg: 2.4; T > Tg: 0.23	Young's Modulus (GPa) Poisson's Ratio 131 0.3 T < Tg: 18.5; T > Tg: 1.2 0.3 T < Tg: 0.92; T > Tg: 0.1 0.3 117 0.34 T < Tg: 3.8; T > Tg: 0.125 0.3 T < Tg: 2.4; T > Tg: 0.23 0.3 For x y: 25; For z: 11 For xy 0.11	$ \begin{array}{c ccccccccccccccccccccccccccccccccccc$				

¹Coefficient of Thermal Expansion, ²Glass Transition Temperature

Since there is a high mismatch in CTEs from all materials involved, the new simulation did not include mechanical load, but a more realistic thermal load (Figure 6). This temperature range and cyclic timing are in accordance with the Joint Electron Device Engineering Council (JEDEC) standards, and the maximum temperature surpasses 0.5 T_m.

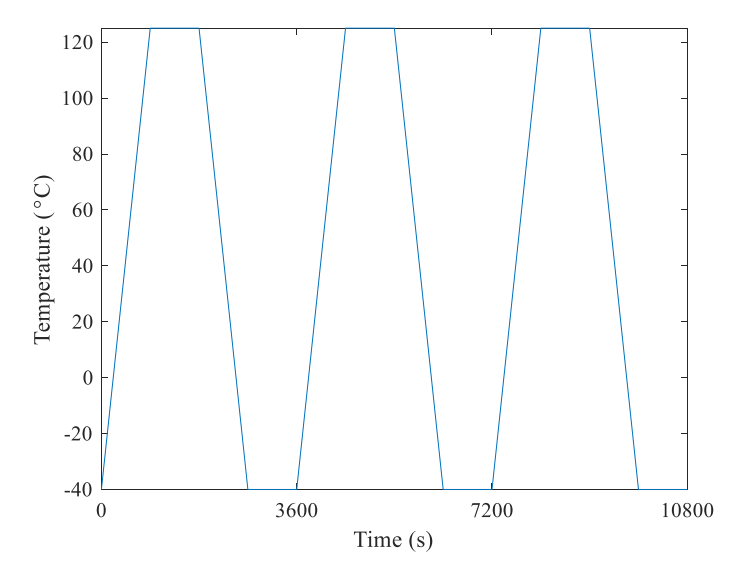


Figure 6. Thermal load.

2.2.2 Results and Discussion

At the end of the third cycle, the nodes with high values of TECS were found to be located at the bottom corners of each solder ball (see Figure 7).

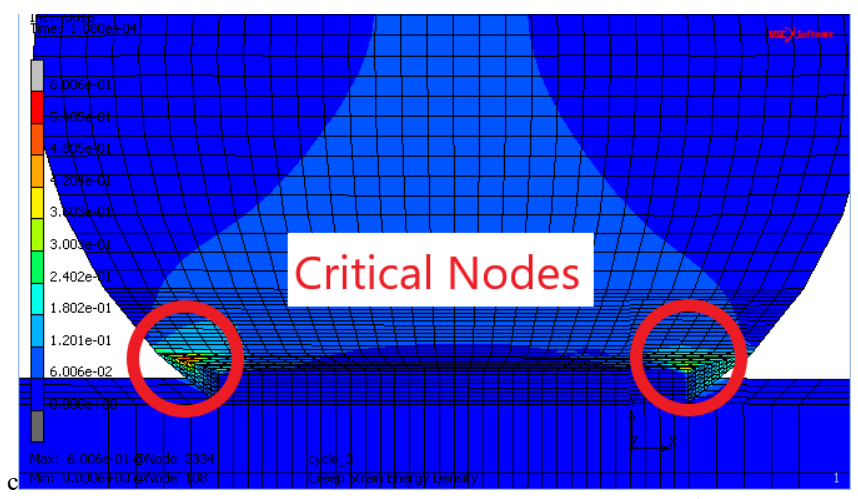
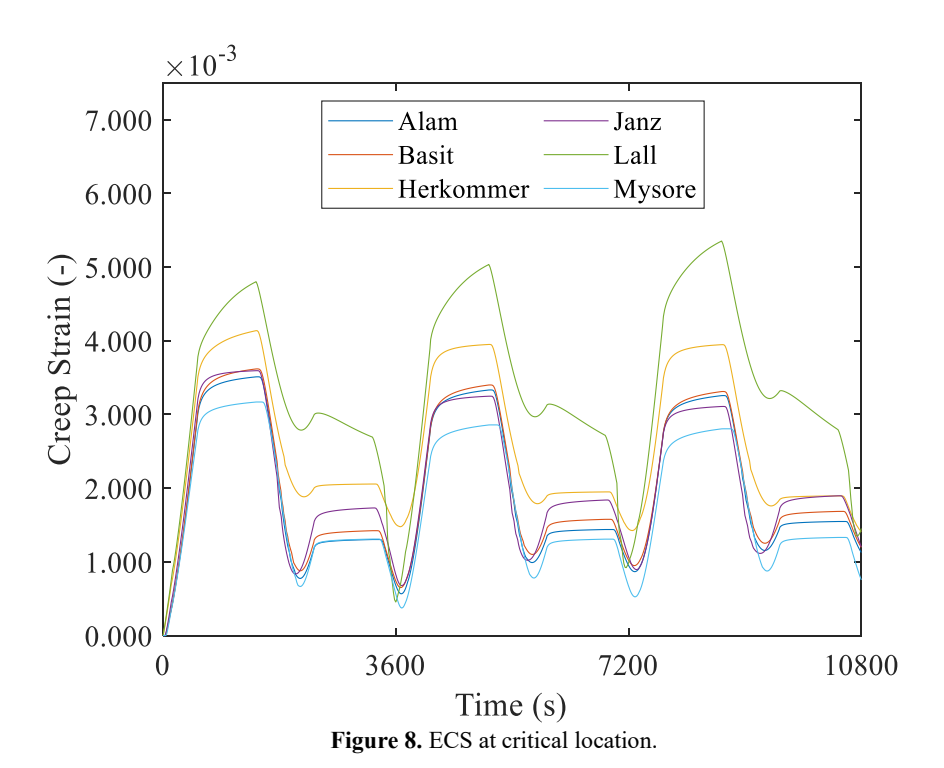


Figure 7. Contour band graph. - TECS distribution at the end of the 3rd thermal cycle.

Three main waves in ECS correspond to the three thermal cycles (Figure 8). There is a considerable similarity during the high-temperature dwell segment. The Alam, Basit, and Janz curves show high agreement during this period. On the other hand, Lall's values align with those of the other authors only at the end of every thermal cycle. Evidently, during the low-temperature dwell segment, all curves display divergent values, except for Herkommer and Janz during the third thermal cycle.



The Creep Strain Energy Density (CSED) vs. time curves from the critical location of each replicate were summarized in Figure 9. It is worth noting that SACQ presents the lowest CSED accumulation among the different soldering materials and the highest expected resolution due to the large number of steps. Additionally, InnoLot and SAC305 curves display a similar

behavior during the first two thermal cycles. Nevertheless, the approximation of the average of CSED only considers the CSED subtraction between the third and second thermal cycle (Table 10).

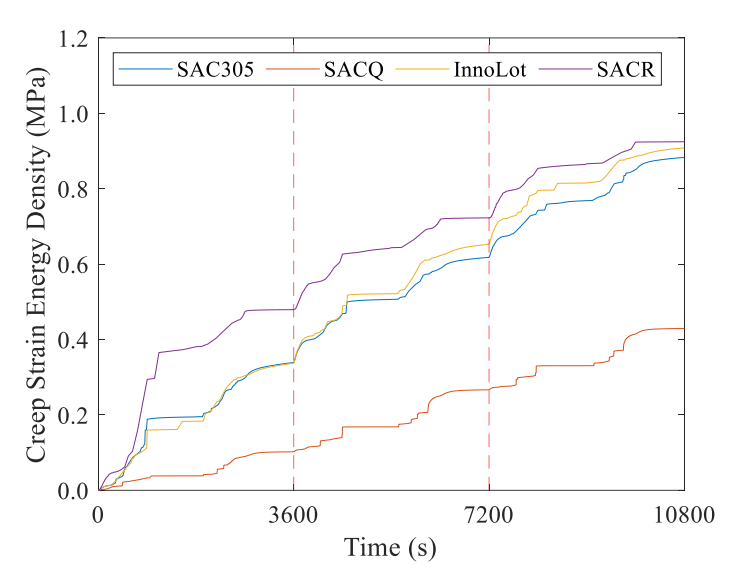


Figure 9. Creep Strain Energy Density Comparison.

Table 10. Approximation of the Average of Creep Strain Energy Density (MPa).

CSED	SAC305	SACQ	InnoLot	SACR
Cycle 1	0.339020	0.102072	0.337066	0.479284
Cycle 2	0.617905	0.266476	0.653259	0.722654
Cycle 3	0.883068	0.429206	0.908353	0.924602

2.2.3 Conclusions

Despite differences in the six sets of viscoplastic parameters, all six simulations agreed on the location of the critical node at the conclusion of the three cycles. This comparison has not been found in the extensive literature database examined.

There is a significant difference in the ECS curves during the low-temperature dwell segment (-40°C); however, there is a considerable similarity among four of the six TECS curves (Alam, Basit, Herkommer, and Janz). Since TECS is the cumulative value of ECS, analyzing TECS solely could lead to a misinterpretation regarding a thorough comparison.

Since Alam, Basit, and Herkommer present a significant similarity of curves with a substantial range of time-steps, it is advisable to use the set of viscoplastic parameters that takes the shortest time (Basit) for simulation purposes.

Doped SAC solders are more advantageous than SAC305 solder in terms of working lifetime. The qualitative results suggest that SACQ has a significant advantage in the operational lifetime compared to SACR, InnoLot, and SAC305.

2.3 Chapter 4. Analysis of reliability models and first estimation of reliability indicators

The reliability of ICs subjected to cycling thermal loads has been a core research topic, with thermal fatigue analysis aimed at predicting the number of cycles to failure. Initially, the Distance to the Neutral Point (DNP) was identified as a key parameter; hence, the farthest solder joint from the neutral point of the IC poses a risk due to the highest thermo-mechanical loads and a geometry that limits the size of the packaging and the number of I/Os.

For creep material models, either the hyperbolic-sine law or Anand's type of models are often used. A more detailed list of creep-based material characterization experiments is summarized in Table 11. The authors who used the hyperbolic-sine model stressed the lack of articles reporting Anand's constants.

Table 11. Employed creep and reliability models in highlighted references.

	Creep Mo	Creep Model		Reliability Model		
Author	Hyperbolic Sine	Anand	Morrow	Darveaux	Coffin Manson	
Lui et al.		X	X			
Che	×		X			
Chen	×					
Guven		×		×		
Lin		X	×			
Che and Pang	×		X		×	
Rahangadale et al.		×	×			

2.3.1 Simulation Setup

For the sake of simplicity in geometry, the authors represent the bottom copper pad using a sharp edge. Based on x-ray microscopic inspections, the corner pad can better approximate real microchips with a non-sharp corner (Figure 10). The current chapter proposes two different edges, sharp and fillet.

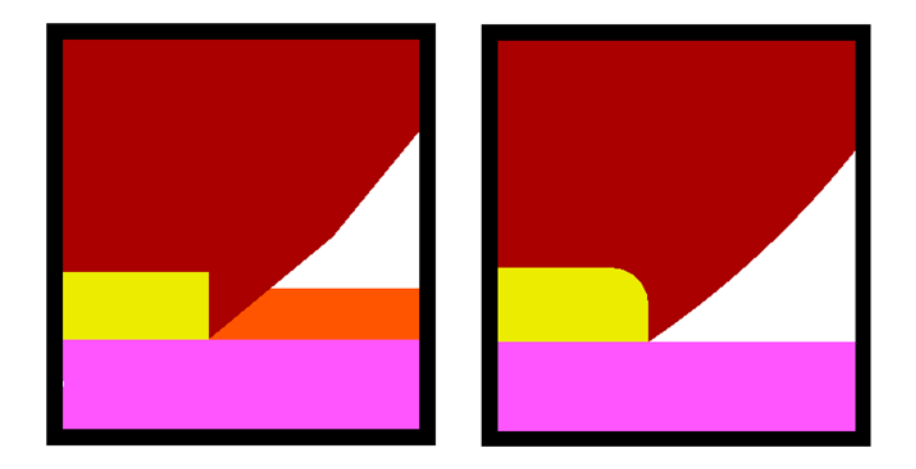


Figure 10. The modelled section: Augmented view of the squared Cu pad profile, and augmented view of the rounded Cu pad profile.

This was the change implemented in the simulation with respect to the section 2.2.1.

2.3.2 Results and Discussion

The contour band graph of the Total Equivalent of Creep Strain (TECS) at the end of the simulation is shown in Figure 11. The node with the highest TECS is located on the outer bottom side of the solder ball. This result agrees with experimental data presented in, where packaging including UBM exhibits cracking initiation in the bottom corners, whereas packages without UBM show cracking initiation in the upper corners.

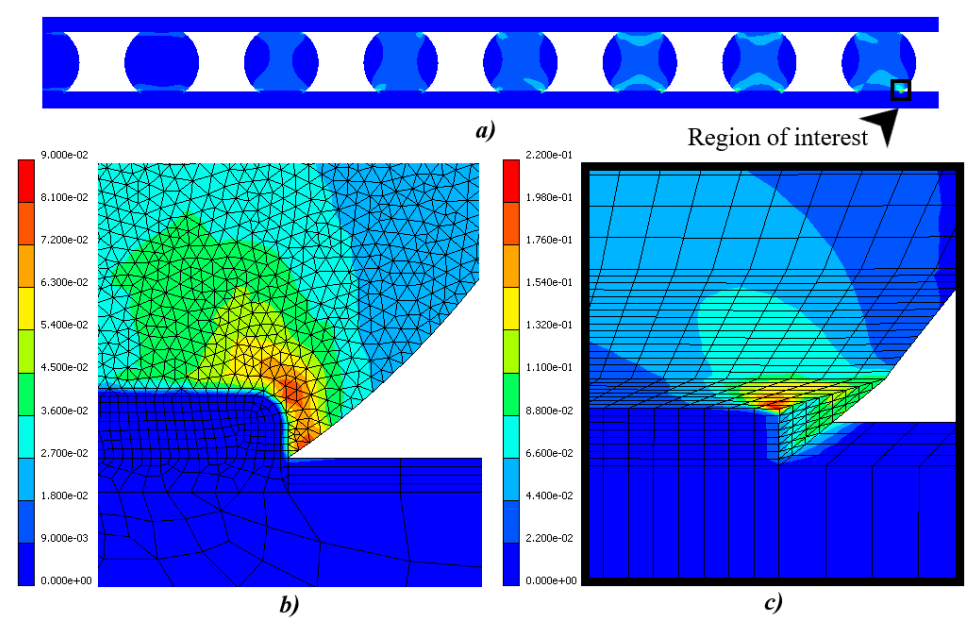


Figure 11. TECS at the end of the three cycles

a) TECS distribution along the solder balls (cropped image), Augmented contour band graph of TECS distribution at the vicinity of the critical node b) rounded Cu pad profile and, c) squared Cu pad profile.

A comparison regarding the copper pad profile was carried out. Since the geometry of the modified model became too complex, the mask layer was neglected following similar study

cases. Creep strain curves (ECS and TECS) from the critical node are presented in Figure 12. Like the squared profile, the location of the critical node remained the same.

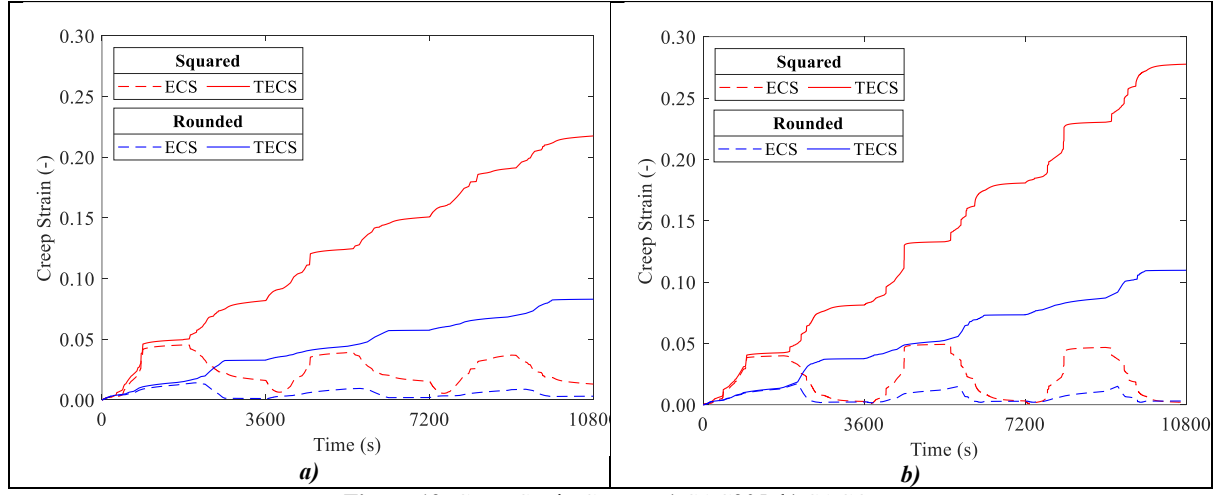


Figure 12. Creep Strain Curves. a) SAC305, b) SACQ.

Following Che and Pang's procedure (subtraction between final values of the third and second cycle), values of the approximation of average strain and energy variation were computed (see Table 12). It should be noticed that all values decreased due to a change in copper pad geometry. High values can be observed for the squared profile, with a significant reduction for the rounded profile.

Table 12 Approximation of the average of creep strain and energy density.

	SAC305		SACQ	
	W_p	$\Delta arepsilon_p$	W_p	$\Delta arepsilon_p$
Squared	0.4738	0.0667	0.0552	0.0968
Rounded	0.1272	0.0255	0.0999	0.0363

2.3.3 Conclusions

The reliability of the solder ball can compromise the functionality of the entire Integrated Circuit. Repetitive thermal loading of a complex FO-WLP package was modeled, varying the copper profile and solder ball material viscoplastic properties. Based on the results, the following conclusion can be drawn in addition the ones mentioned in section **Error! Reference source not found.**:

Solder masks can be neglected in the geometry of the electronic packaging since it does not significantly affect creep results.

A change in the copper pad profile shape (squared to rounded) shows a stress reduction and, therefore, more stable creep curves. Additionally, it accentuates the difference of creep values between materials by nearly 16% regarding creep strain values.

A filet copper pad edge might seem advantageous; however, it greatly impacts the mesh complexity. Therefore, a longer simulation time is required, and special attention should be paid to unlinking nodes.

Since reliability models are inversely related to inelastic strain energy, SACQ presented the most promising working time, followed by SACR, Innolot, and SAC305 in that order.

2.4 Chapter 5. Efficient modeling framework for estimation of reliability indicators

A computational cost-effective modeling framework is proposed in the present work, a simple and efficient tool that can be applied for extensive parameter studies for solder interconnect analysis. A Fan Out—Wafer Level Packaging (FO-WLP) model was built and analyzed using multiple simulation replicates in a thermal testing environment to evaluate geometry-related modeling aspects; and materials-related modeling aspects. Four main parameters were contemplated for a comprehensive comparison.

- (1) Regarding the solder materials, SAC305 and SACQ were selected for the analysis. A critical location of the model is the bond pad edge, which is prone to induce stress concentrations with ideal sharp edges, while real geometry is often blunt [115], [134].
- (2) Therefore, a model geometry with a chamfered bond pad edge was built and compared to the sharp edge configuration in the simulations.
- (3) A pseudo-3-D modeling domain was also constructed from the previous 2-D model to employ a combined plane strain plane stress analysis to improve the accuracy without compromising computational costs.
- (4) Finally, the effect of incorporating thin IMC layers was analyzed, contrasting with simulations that dismiss IMC layers.

The impact of the parameter variations was evaluated on the creep strain and creep strain energy densities presented in the results section, together with the analyses of von Mises and shear stresses in the critical locations of the solder. Reliability prediction for low cycle fatigue requires strain or strain energy-based reliability indicators; furthermore, an averaging scheme, which was proposed in this work, is dedicated to the modeling framework.

2.4.1 Simulation Setup

Bond pad edges are often modeled with idealized sharp edges. In contrast, real geometries, as shown in Scanning Electron Microscopy (SEM) images, may become blunt in the final assembly due to the patterning process steps. The edge shape can strongly influence stress distributions in the solder balls; hence, two different edge shapes were proposed in this study: sharp and blunt (chamfered), as shown in Figure 13. The chamfer dimensions are: 4 μm at 45°. Additionally, two extra layers were optionally included to analyze the variation related to IMC formation at the bond pad–solder interface. An estimated 10% of the copper pad's total thickness, 2 μm, was established for each IMC layer's (Cu₆Sn₅ and Cu₃Sn) thickness with idealized smooth geometries at the interfaces.

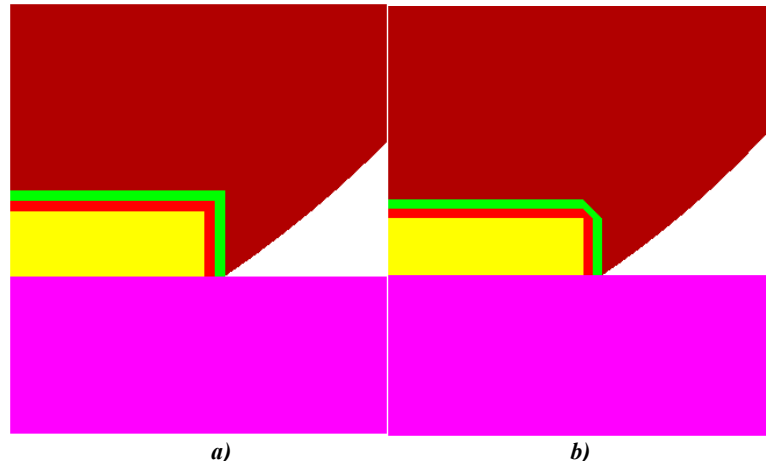


Figure 13. Modeled cross-section of the FO-WLP package.

a) ideal, and b) real geometry.

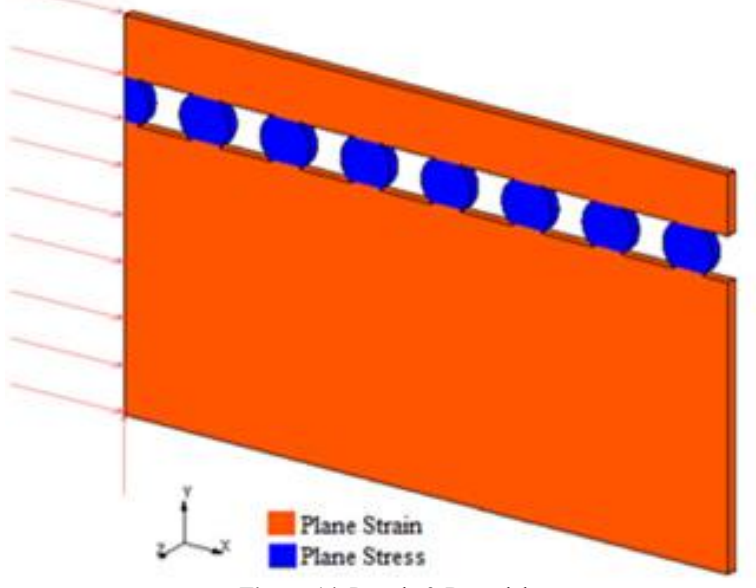


Figure 14. Pseudo 3-D model Combined plane strain and plane stress conditions.

A 2-D model allows employment of a fine mesh, which can lead to a more accurate local distribution of results with low computational costs. For the simulation domain, therefore, a 2-D cross-section was modeled in this work, either with 2-D elements with a plane strain condition or with a pseudo-3-D variation, using a linear geometry extension in the out-of-plane direction (Figure 14). This pseudo-3-D approach allows the model of the solder with plane stress condition, whereas the other parts of the assembly may remain in plane strain condition. Therefore, overestimations of the stresses in the solder balls, which often arise in pure plane strain conditions, are avoided.

We have chosen to neglect the residual stresses in the solder at the start of the thermal testing. Based on similar studies, the initial temperature was set at 26 °C, ramp rates were 11 °C/min, and the hold times were 15 min. The isothermal load applied to all the nodes in the model is shown in Figure 15.

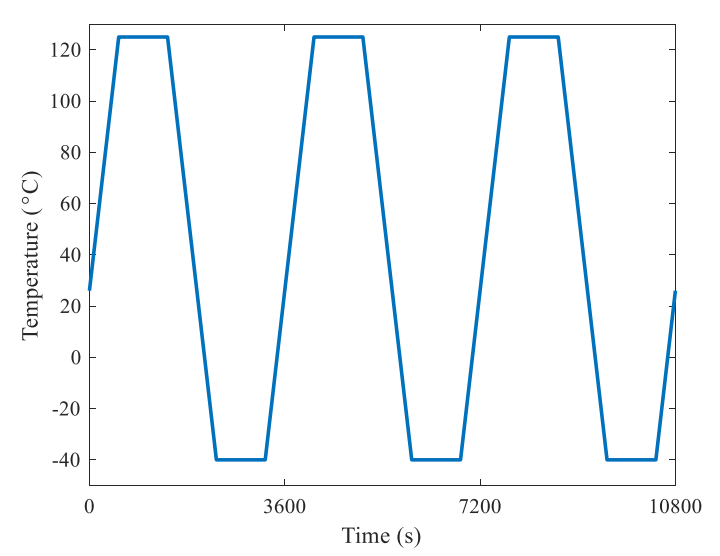


Figure 15. Applied temperature load as a function of time.

2.4.2 Results and Discussion

In Table 13, both fatigue indicators \triangle CSED and \triangle TECS are listed for all calculated cases. The table is organized by the simulation domains in the columns 2-D and pseudo-3-D cases, which represent the lower and upper bound for the strain and strain energy-related values, respectively. The higher confinement by the plane strain condition 2-D restricts strains and strain energies, while less confinement in the pseudo-3-D case with the plane stress condition for the solder allows higher strains and, therefore, higher strain energies. In a real scenario, these indicators will fall in between the bounds; hence, the averages are displayed in the third

column, and further analysis and conclusions will be based on these average values. In a full 3-D simulation, a volume-averaging scheme would be required for accurate indicators.

In terms of material quality, these reliability indicators alone would not provide a valid basis for comparison, as the number of cycles to fracture will also depend on the fatigue ductility coefficient and fatigue exponents. Therefore, sound conclusions cannot be drawn by comparing average $\Delta TECS$ or $\Delta CSED$ between the dissimilar material qualities of SAC305 and SACQ. While the lower average $\Delta TECS$ for SACQ would indicate better fatigue response, average $\Delta CSED$ shows the opposite trend, and the reason is that the strength of SACQ is higher; therefore, the lower strain parameter, while with less deformation, stresses increase, resulting in high strain energy parameters. By calculating the number of cycles to failure, the high-reliability performance of SACQ can be shown.

The effect of the IMC incorporation over the Cu bond pad in the simulations shows only minor differences in the fatigue parameters for the solder. Here, IMC will further enforce the already relatively high strength Cu pad at the solder interface, decreasing deformation slightly in the close vicinity of the pad within the solder as shown by the decrease in $\Delta TECS$ values, while stress has less effect; therefore, strain energy density and $\Delta CSED$ will also slightly decrease with a few percent.

The advantage of the realistic bond pad geometry in the simulation can be seen in the decreased Δ CSED values for blunt edges compared to the ideal sharp-edged geometries.

2-D Pseudo-3-D Average (Lower Bound) (Upper Bound) (2-D-Pseudo-3-D) ΔCSED ΔCSED ΔCSED SAC305 ΔTECS ΔTECS **ΔTECS** (MPa) (MPa) (MPa) w/o IMC 0.0133 0.3105 0.0094 0.2101 0.0114 0.2603 Sharp w/ IMC 0.3016 0.0093 0.25460.01280.2075 0.0111 w/o IMC 0.0145 0.3306 0.0086 0.0116 0.2570 0.1833 Blunt w/ IMC 0.0082 0.0113 0.2498 0.0143 0.3263 0.1732 ΔCSED ΔCSED ΔCSED **SACQ** ΔTECS ΔTECS **ΔTECS** (MPa) (MPa) (MPa) w/o IMC 0.0105 0.4308 0.00750.2979 0.0090 0.3644 Sharp w/IMC 0.00760.0089 0.3589 0.0101 0.41760.3001 w/o IMC 0.0116 0.4622 0.0038 0.0743 0.0077 0.2683 Blunt w/ IMC 0.4528 0.0037 0.0076 0.0114 0.0037 0.2612

Table 13 Summary of study cases.

2.4.3 Conclusions

The usability of the reliability indicators shows predictions are sound with the energy-based parameter (Δ CSED average) but may be fallacious with the purely strain-based one due to

strain (or stress) alone is not sufficient in temperature-dependent cases. The following conclusions are drawn related to the essential modeling elements:

1. Efficient planar simulation framework with 2-D and pseudo-3-D meshed geometries

provides a quick estimate for lower and an upper bound for the strain, stress and strain energy-

related parameters, respectively. In a real scenario, these indicators will fall in between the

calculated bounds. This calculation framework can be employed for extensive parameter

studies solved rapidly at low computational costs.

2. In terms of material quality, simulation results provide a sound insight into the behavior

of the structure, showing the stiffer behavior of SACQ compared to SAC305. Nevertheless, the

reliability indicators alone would not provide a valid basis for comparison of dissimilar solders,

as the number of cycles to fracture will also depend on the fatigue ductility coefficient and

fatigue exponents.

The effect of the IMC incorporation over the Cu bond pad in the simulations shows 3.

only minor differences in the fatigue parameters for the solder. IMC will further enforce the

already relatively high-strength Cu pad at the solder interface, decreasing deformation slightly

in the close vicinity of the pad within the solder.

4. Related to the bond pad geometries, the advantage of the realistic blunt bond pad

geometry in the simulation is obviously lowering stresses. In the worst scenario, fatigue

parameters can be overestimated by over 30% with the ideal sharp-edged geometries.

Summary of New Scientific Results

The dissertation findings are summarized in four thesis points. The author's works in which the

actual thesis points were published are in square brackets.

Thesis 1 [Publication: J1 and C1]

A virtual test bench was developed that is tailored for strain analysis in solder interconnects.

Evaluating lead-free (Sn-3.5Ag, SAC305, SAC387) and SnPb solder behavior in the simplified

soldered stack, which was subjected to simulated thermal and mechanical loads in the test

bench environment, showed a significant reduction in creep deformations for lead-free solders.

It was found that among the lead-free solders, SAC305 exhibits the most favorable

performance due to its lower average creep strain, indicating superior mechanical stability

under thermal and mechanical loads.

17

Thesis 2 [Publication: C2 and C3]

Methodology was developed for the evaluation of the goodness of material parameters for simulations of advanced electronic packaging subjected to thermal loads. Out of the six selected Anand solder creep parameter sets describing SAC305, it was found that the favorable set provided accurate and computationally stable simulation results, as evaluated by creep strain and creep strain energy densities, at the lowest computational costs. Additionally, doped SAC solders (SACQ, SACR, InnoLot) showed improved creep strain energy density in the simulations, with SACQ being beneficial due to its lower average creep strain energy density.

Thesis 3 [Publication: J2]

A test bench was developed to evaluate the simplifications of the modeled geometry for interconnects in advanced packaging. Solder—solder pad geometries were examined by varying contact pad edges (fillet, chamfer, and sharp) for Fan-Out Wafer-Level Packaging. It was found that slight changes in geometry reduce stress and thus accentuate differences in creep behavior among soldering materials. Fillet-shaped copper pads resulted in a 16% reduction in creep strain energy density in the contacting solder, which can significantly impact reliability predictions.

Thesis 4 [Publication: J3]

An efficient finite element calculation framework was developed for modeling deformation and predicting the lifetime of solder interconnects in advanced packaging under cyclic thermal loads. Within this simulation framework, planar 2-D and pseudo-3-D meshed geometries provide quick estimates for lower and upper bounds of strain, stress, and strain energy-related parameters. Reliability prediction for low cycle fatigue also requires an averaging scheme that provides reliability indicators. This scheme, proposed in this work, is dedicated to the modeling framework. It was found that the usability of the reliability indicators is sound with the energy-based parameter but may be misleading with the purely strain-based one, as strain (or stress) alone is insufficient in temperature-dependent cases. This calculation framework can be employed for extensive parameter studies, solved rapidly at low computational costs.

4. List of Publications

4.1 Articles in internationally reviewed academic journals.

- [J1] R. S. Vargas Cruz and V. Gonda, "Comparison of creep behavior for lead free solders Sn-3.5Ag, SAC305 and SAC387," Banki Reports, vol. 2, no. 2, pp. 16–21, 2019, [Online]. Available: http://bk.bgk.uni-obuda.hu/index.php/BK/article/view/101
- [J2] R. S. Vargas Cruz and V. Gonda, "Creep and Reliability Prediction of a Fan-Out WLP Influenced by the Visco-Plastic Properties of the Solder," Acta Polytechnica Hungarica, vol. 19, no. 7, pp. 235–254, 2022, doi: 10.12700/APH.19.7.2022.7.13.
- [J3] R. S. Vargas Cruz and V. Gonda, "Efficient Modeling Framework for FO-WLP Solder Interconnect Behavior During Thermal Cycling," Metals (Basel), vol. 15, no. 1, p. 17, Dec. 2024, doi: 10.3390/met15010017

4.2 Papers at international scientific conferences.

- [C1] R. S. V. C and V. Gonda, "Comparison of the thermal-mechanical behavior of a soldered stack influenced by the choice of the solder," in 2019 20th International Conference on Thermal, Mechanical and Multi-Physics Simulation and Experiments in Microelectronics and Microsystems (EuroSimE), IEEE, Mar. 2019, pp. 1–6. doi: 10.1109/EuroSimE.2019.8724590.
- [C2] R. S. Vargas Cruz and V. Gonda, "Solder joint reliability based on creep strain energy density for SAC305 and doped SAC solders," MATEC Web of Conferences, vol. 343, p. 02005, Aug. 2021, doi: 10.1051/matecconf/202134302005.
- [C3] R. S. Vargas C and V. Gonda, "Sensitivity of the structural behavior of SAC305 interconnects on the variations of creep parameters," in 2021 IEEE 15th International Symposium on Applied Computational Intelligence and Informatics (SACI), IEEE, May 2021. doi: 10.1109/SACI51354.2021.9465551.